

# The neutron skin of $^{208}\text{Pb}$ and the density dependence of the symmetry energy

Francesca Sammarruca and Pei Liu

Physics Department, University of Idaho, Moscow, ID 83844, U.S.A

## Abstract

We explore neutron skin predictions for  $^{208}\text{Pb}$  in relation to the symmetry pressure in various microscopic models based on realistic nucleon-nucleon potentials and either the Dirac-Brueckner-Hartree-Fock approach or the conventional Brueckner-Hartree-Fock framework implemented with three-body forces. We also discuss the correlation between the neutron skin and the radius of a fixed-mass neutron star.

PACS number(s): 21.65.+f, 21.30.Fe

## 1 Introduction

Microscopic predictions of the nuclear equation of state (EoS), together with empirical constraints from EoS-sensitive observables, are a powerful combination to learn about the in-medium behavior of the nuclear force. With this objective in mind, over the past several years, our group has taken a broad look at the EoS exploring diverse aspects and extreme states of nuclear matter.

From the experimental side, intense effort is going on to obtain reliable empirical information for the less known aspects of the EoS. Heavy-ion (HI) reactions are a popular way to seek constraints on the symmetry energy, through analyses of observables that are sensitive to the pressure gradient between nuclear and neutron matter. Isospin diffusion data from HI collisions, together with analyses based on isospin-dependent transport models, provide information on the slope of the symmetry energy. Naturally, different reaction conditions, in terms of energy per nucleon and/or impact parameter, will probe different density regions.

Concerning the lower densities, isospin-sensitive observables can also be identified among the properties of normal nuclei. The neutron skin of neutron-rich nuclei is a powerful isovector observable, being sensitive to the slope of the symmetry energy, which determines to which extent neutrons are “pushed out” to form the skin. It is the purpose of this note to systematically examine and discuss the symmetry energy properties in microscopic models and the corresponding neutron skin predictions. We will take the skin of  $^{208}\text{Pb}$  as our representative isovector “observable”.

Parity-violating electron scattering experiments are now a realistic option to determine neutron distributions with unprecedented accuracy. The neutron radius of  $^{208}\text{Pb}$  is expected to be measured within 0.05 fm thanks to the electroweak program

at the Jefferson Laboratory [1]. This level of accuracy could not be achieved with hadronic scattering due to the large theoretical uncertainties present in all hadronic models. Parity-violating electron scattering at low momentum transfer is especially suitable to probe neutron densities, as the  $Z^0$  boson couples primarily to neutrons. With the success of this program, reliable empirical information on neutron skins will be able to provide, in turn, much needed *independent* constraint on the density dependence of the symmetry energy.

Furthermore, with the Facility for Rare Isotope Beams (FRIB) recently approved for design and construction at Michigan State University, studies of neutron-rich systems become particularly important and timely. Such program will have widespread impact, reaching from the physics of exotic nuclei to nuclear astrophysics.

## 2 Predictions of neutron densities with a simple energy functional

We calculate proton and neutron density distributions with a method described in an earlier work [2]. Namely, we use an energy functional based on the semi-empirical mass formula, where the volume and symmetry terms are contained in the isospin-asymmetric equation of state. Thus, we write the energy of a (spherical) nucleus as

$$E(Z, A) = \int d^3r e(\rho(r), \alpha(r))\rho(r) + \int d^3r f_0(|\nabla\rho(r)|^2 + \beta|\nabla\rho_I(r)|^2) + \text{Coulomb term.} \quad (1)$$

In the above equation,  $\rho$  and  $\rho_I$  are the usual isoscalar and isovector densities, given by, (in terms of the neutron and the proton densities),  $\rho_n + \rho_p$  and  $\rho_n - \rho_p$ , respectively,  $\alpha$  is the neutron asymmetry parameter,  $\alpha = \rho_I/\rho$ , and  $e(\rho, \alpha)$  is the energy per particle in isospin-asymmetric nuclear matter. We use realistic nucleon-nucleon forces, (specifically, Bonn B [3]), and our latest EoS from Ref. [4]. The latter is based on the Dirac-Brueckner-Hartree-Fock method, the technical framework of which was described earlier [5]. The energy per particle in symmetric and neutron matter are shown in Fig. 1.

From fits to nuclear binding energies, the constant  $f_0$  in Eq. (1) is approximately  $70 \text{ MeV fm}^5$ , whereas the contribution of the term proportional to  $\beta$  was found to be minor [6]. Thus we will neglect it. (The magnitude of  $\beta$  was estimated to be about  $1/4$  in Ref. [7], where it was observed that, even with variations of  $\beta$  between  $-1$  and  $+1$ , the effect of the  $\beta$  term on the neutron skin was negligibly small.)

The parameters of the proton and neutron density functions are obtained by minimizing the value of the energy, Eq. (1), assuming Thomas-Fermi distributions. Although simple, this method has the advantage of allowing a very direct connection between the EoS and the properties of finite nuclei. (It could be used, for instance, to determine a semi-phenomenological EoS by fitting to both binding energies and

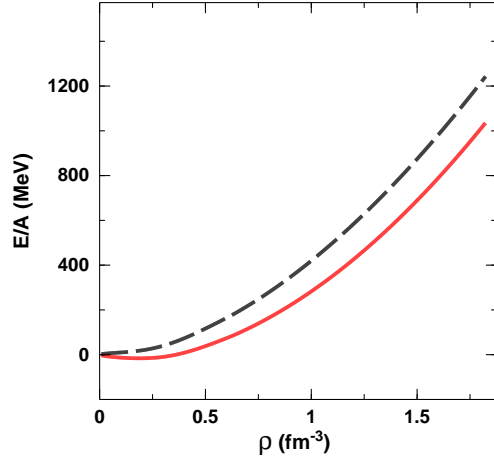


Figure 1: (color online) Energy/particle in symmetric matter (solid red) and neutron matter (dashed black) as from our latest DBHF calculations.

charge radii of closed-shell nuclei.)

In Fig. 2, we show the proton and neutron Thomas-Fermi distributions for  $^{208}\text{Pb}$  as obtained with the method describe above and the DBHF model for the EoS. The predicted proton and neutron root-mean-square radii are 5.39 fm and 5.56 fm, respectively.

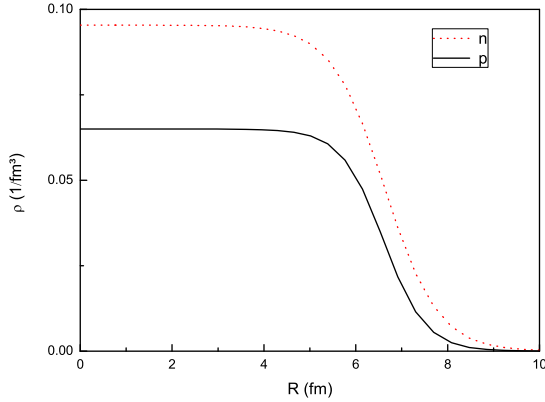


Figure 2: (color online) Neutron (red) and proton (black) point densities as obtained from the DBHF model.

### 3 Symmetry pressure, neutron skin, and neutron star radii in microscopic models

Typically, predictions of the symmetry energy at saturation density encountered in the literature are in reasonable agreement with one another, ranging approximately from 26 to 35 MeV. On the other hand, the slope of the symmetry energy is more model dependent. This is seen through the symmetry pressure, defined as

$$L = 3\rho_0 \left( \frac{\partial E_{sym}(\rho)}{\partial \rho} \right)_{\rho_0} \approx 3\rho_0 \left( \frac{\partial e_{n.m.}(\rho)}{\partial \rho} \right)_{\rho_0}. \quad (2)$$

Thus,  $L$  is sensitive to the gradient of the energy per particle in neutron matter ( $e_{n.m.}$ ). Clearly, the neutron skin, given by

$$S = \sqrt{\langle r_n^2 \rangle} - \sqrt{\langle r_p^2 \rangle}, \quad (3)$$

is highly sensitive to the same gradient.

Values of  $L$  are reported to range from -50 to 100 MeV as seen, for instance, through the numerous parametrizations of Skyrme interactions (see Ref. [8] and references therein), all chosen to fit the binding energies and the charge radii of a large number of nuclei. Heavy-ion data impose boundaries for  $L$  at  $85 \pm 25$  MeV [9, 10]. Also, a nearly linear correlation is observed between the neutron skin  $S$  and the  $L$  parameter, see Fig. 3. (The shown correlation is taken from Ref. [11].) More stringent constraints are being extracted [12].

Such phenomenological studies are very useful, but, ultimately, *ab initio* approaches must be employed in order to get true physical insight. By *ab initio*, we mean that the starting point is a realistic two-body potential, possibly complemented by three-body forces. The tight connection with the underlying two-body potential will then facilitate the physical understanding, when combined with reliable constraints.

Our model does not include three-body forces (TBF) explicitly, but incorporates the class of TBF originating from the presence of nucleons and antinucleons (the “Z-diagrams”), which are effectively accounted for in the DBHF scheme [13].

As the other main input of our comparison, we will take the EoS’s from the microscopic approach of Ref. [14]. There (and in previous work by the authors), the Brueckner-Hartree-Fock (BHF) formalism is employed along with microscopic three-body forces. However, in Ref. [14] the meson-exchange TBF are constructed applying the same parameters as used in the corresponding nucleon-nucleon (NN) potentials, which are: Argonne V18 (V18, [15]), Bonn B (BOB, [3]), Nijmegen 93 (N93, [16]). The popular (but phenomenological) Urbana TBF (UIX, [17]) is also utilized in Ref. [14]. Convenient parametrizations in terms of simple analytic functions are given in all cases and we will use those to generate the various EoS’s. We will refer to this approach, generally, as “BHF + TBF”.

In Fig. 4, we display our DBHF predictions for the symmetry energy, solid black curve, along with those from V18, BOB, UIX, and N93. All values of the symmetry

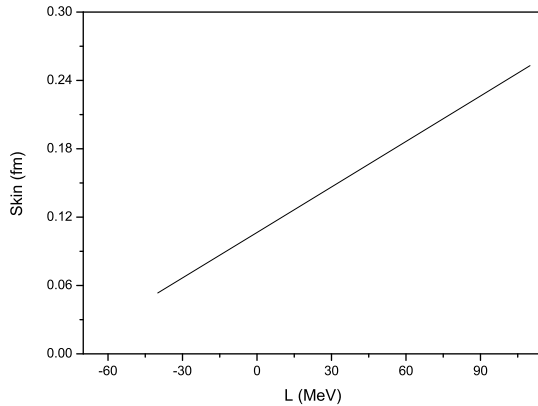


Figure 3: (color online) Relation between the neutron skin in  $^{208}\text{Pb}$  and the  $L$  parameter as found in Ref. [11].

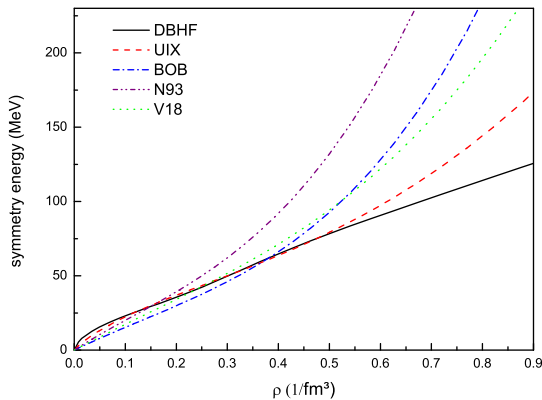


Figure 4: (color online) Predictions for the symmetry energy from DBHF and various “BHF + TBF” models considered in the text.

energy at the respective saturation densities are between 29 and 34 MeV. A larger spreading is seen in the  $L$  parameter, see Fig. 5, where the values range from about 70 to 106 MeV. The respective neutron skin predictions are shown on the vertical axis.

We notice that all BHF+TBF models predict larger  $L$ , and thus larger neutron skins, compared to DBHF, corresponding to a faster growth of the energy per particle in neutron matter relative to symmetric matter. This can be seen in Fig. 4, especially for the higher densities. The present calculations reveal that there are more subtle, but significant differences at low to medium densities as well. We recall that, in our DBHF calculation, the growth of the symmetry energy (especially at high density) is moderated by the repulsive and strongly density dependent “Dirac” effect, which impacts all partial waves and, in particular, the  $T=0$  partial waves, absent in neutron matter [4].

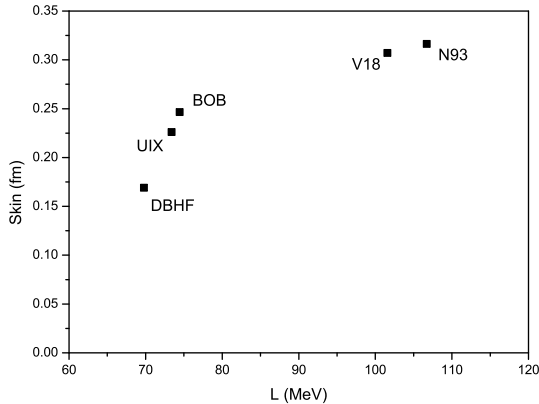


Figure 5: (color online) Neutron skin of  $^{208}\text{Pb}$  *vs.* the symmetry pressure energy for the models considered in the text.

The next term in the expansion of the symmetry energy is the  $K_{sym}$  parameter,

$$K_{sym} = 9\rho_0^2 \left( \frac{\partial^2 E_{sym}(\rho)}{\partial \rho^2} \right)_{\rho_0}, \quad (4)$$

which is a measure for the curvature of the symmetry energy. The neutron skin *vs.*  $K_{sym}$  is shown in Fig. 6 for the various models. Although the values of  $K_{sym}$  appear more spread out, the large negative values obtained with some of the parametrizations of the Skyrme model are not present. Those large negative values (as low as -600 MeV) produced by Skyrme models indicate a strongly downward curvature already at low to medium densities. We also notice from Fig. 6 that no clear correlation can be identified between  $K_{sym}$  and the neutron skin.

Going back to the correlation between neutron skin and symmetry pressure, we now wish to further explore the nature of such correlation. For that purpose, we made the following test: from our baseline DBHF model, we applied *ad hoc* variations of the symmetry energy *only*, leaving the symmetric matter EoS unaltered. Specifically, we increased the symmetry energy in small steps, by an amount between 5% and 20%, and recalculated the neutron skin of  $^{208}\text{Pb}$  for each of these “varied models”. (Note that the charge radius didn’t change in any significant manner as a result of these modifications.) The corresponding skin- $L$  correlation is much closer to a linear one, compare Fig. 5 and Fig. 7. The actual models considered in Fig. 5 are quite different from one another, in both the symmetric matter EoS and the symmetry energy. And, although the general pattern is that larger  $L$  corresponds to larger neutron skin, the

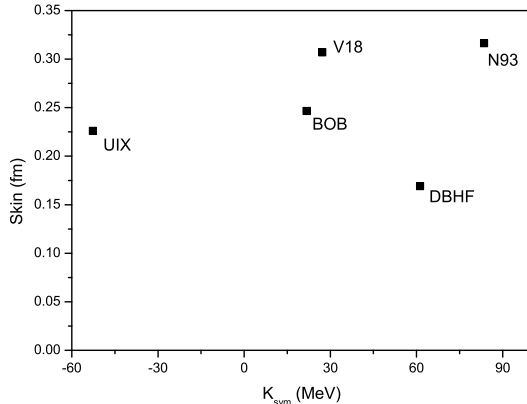


Figure 6: (color online) Neutron skin of  $^{208}\text{Pb}$  *vs.* the curvature of the symmetry energy,  $K_{sym}$ , for the models considered in the text.

actual relation is more complex, as the r.m.s. radius of the neutron distribution will also receive feedback from the smaller or larger degree of attraction which binds the neutrons to the protons and which is determined by the symmetric matter EoS.

We conclude this section by showing in Fig. 8 the relation between the neutron skin of  $^{208}\text{Pb}$  and the radius of a  $1.4M_{\odot}$  neutron star for the models shown in Fig. 5. (For simplicity, we consider here only pure neutron matter.) At first, the figure can appear surprising, since larger skin does not necessarily imply larger radius. On the other hand, one must keep in mind that: 1) The radius depends mostly on the pressure at the higher densities, whereas the skin probes normal or subnuclear densities; 2) As we argued in the previous paragraph for the case of a nucleus, these models differ from one another in more than just the slope of the symmetry energy.

Table 1: Radii and central energy densities of a  $1.4M_{\odot}$  neutron star predicted by each model.

Model	R(km)	$e_c$ ( $10^{14}\text{gm/cm}^3$ )
DBHF	12.4	6.5
UIX	11.8	9.05
V18	12.3	6.89
BOB	12.4	6.16
N93	13.0	5.91

Table I can give additional insight. Even though UIX predicts a larger skin than DBHF, its predicted neutron star radius is 11.8 km as opposed to 12.4 km from DBHF. Notice, however, the much larger central energy density in the UIX case. In other words, UIX produces a more compact  $1.4M_{\odot}$  neutron star. BOB and V18 are quite similar to DBHF in both radius and central energy density. On the other hand,

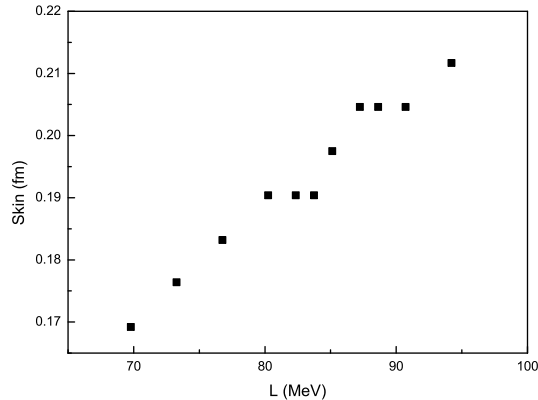


Figure 7: (color online) The relation between the neutron skin of  $^{208}\text{Pb}$  and the symmetry pressure for the DBHF model and *ad hoc* variations of the symmetry energy as explained in the text.

in a case like N93, where, as seen from Fig. 4, high pressure is sustained pretty much at all densities, the  $1.4M_{\odot}$  star is larger and more diffuse. In summary, for each model the available mass will distribute itself differently, depending on both the symmetric and the asymmetric part of the EoS *at each relevant density*. The different values of the predicted maximum masses, apparent from Fig. 9, reflect differences among the models in their symmetric matter EoS's.

To complete this test, we took again the arbitrarily varied “models” used in Fig. 7 and reexamined the radius *vs.*  $L$  (or *vs.* neutron skin) relation, see Figs. 10 and 11. The correlations are nearly linear. For completeness, the mass-radius relation for these varied “models” is displayed in Fig. 12, and shows that the same maximum mass is predicted in all cases (as expected, since the symmetric matter EoS is unchanged).

## 4 Outlook

The neutron skin is an important isospin-sensitive “observable” which is essentially determined by the difference in pressure between symmetric and neutron matter. Interesting correlations can be established between the skin of a heavy nucleus (e. g.  $^{208}\text{Pb}$ ) and neutron star properties [1]. We calculated the neutron skin of  $^{208}\text{Pb}$  with our latest EoS based on the DBHF approach [4], as well as other EoS's based on BHF calculations with TBF, with the parameters of the meson-exchange TBF consistent with those of the underlying meson-exchange NN potential.



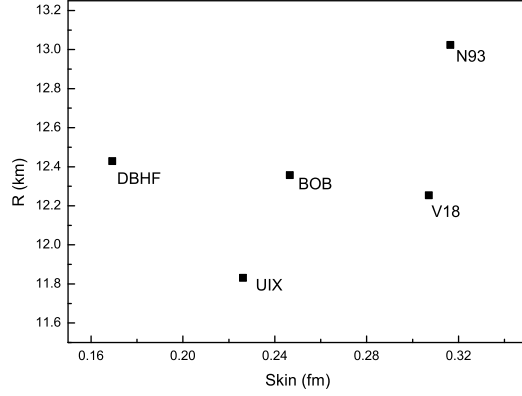


Figure 8: (color online) Neutron skin of  $^{208}\text{Pb}$  *vs.* the radius of a  $1.4M_{\odot}$  neutron star for the models considered in the text.

Most models agree on the value of  $E_{sym}$  around the saturation point within a few MeV, but we are far from a reasonable agreement on the slope of the symmetry energy and even farther from agreement on the curvature. Although microscopic models do not display as much spread as phenomenological ones, a point that comes out clearly from the present study is that a measurement of the neutron skin of  $^{208}\text{Pb}$  with an accuracy of 0.05 fm, as it has been announced [18], should definitely be able to discriminate among EoS's from microscopic models.

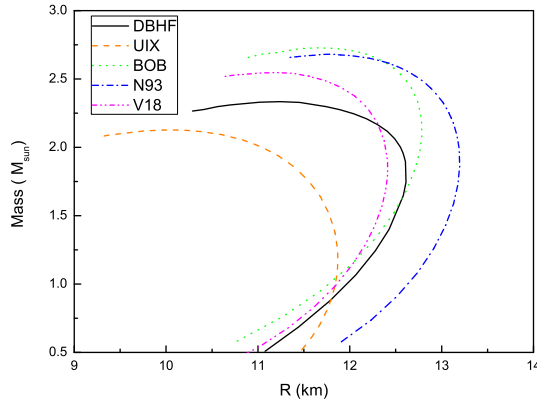


Figure 9: (color online) Neutron star mass-radius relation for the models considered in the text.

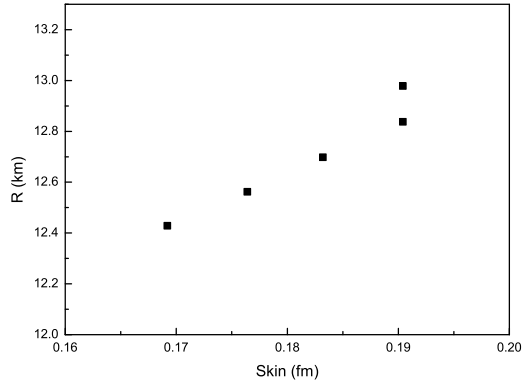


Figure 10: (color online) Neutron skin of  $^{208}\text{Pb}$  *vs.* the radius of a  $1.4M_{\odot}$  neutron star for the DBHF model and *ad hoc* variations as explained in the text.

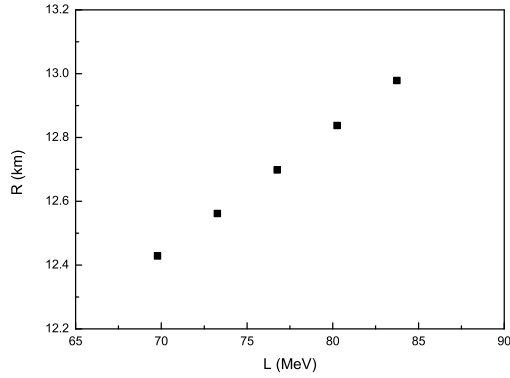


Figure 11: (color online) The symmetry pressure,  $L$ , *vs.* the radius of a  $1.4M_{\odot}$  neutron star for the DBHF model and *ad hoc* variations as explained in the text.

## Acknowledgments

Support from the U.S. Department of Energy under Grant No. DE-FG02-03ER41270 is acknowledged.

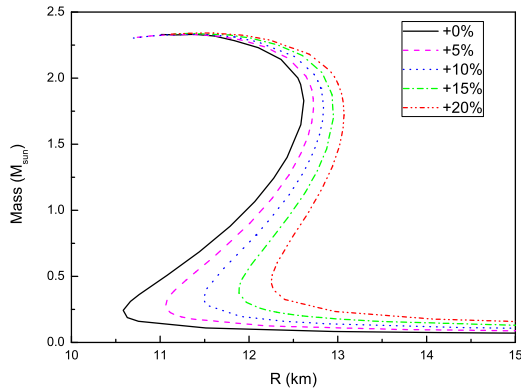


Figure 12: (color online) Neutron star mass-radius relation for the DBHF model and *ad hoc* variations as explained in the text. The legend on the upper right corner indicates the amount by which the symmetry energy has been increased in each case.

## References

- [1] J. Piekarewicz, arXiv:nucl-th/0607039, and references therein.
- [2] D. Alonso and F. Sammarruca, Phys. Rev. C **68**, 054305 (2003).
- [3] R. Machleidt, Adv. Nucl. Phys. **19**, 189 (1989).
- [4] F. Sammarruca and Pei Liu, arXiv:0806.1936 [nucl-th].
- [5] D. Alonso and F. Sammarruca, Phys. Rev. C **67**, 054301 (2003).
- [6] K. Oyamatsu *et al.*, Nucl. Phys. **A634**, 3 (1998).
- [7] R.J. Furnstahl, Nucl. Phys. **A706**, 85 (2002).
- [8] B.A. Li and L.W. Chen, Phys. Rev. C **72**, 064611 (2005).
- [9] L.W. Chen *et al.*, arXiv:0711.1714 [nucl-th].
- [10] Pawel Danielewicz and Jenny Lee, arXiv:0708.2830 [nucl-th].
- [11] Lie-Wen Chen, Che Ming Ko, and Bao-An Li, arXiv:nucl-th/0509009.
- [12] M.B. Tsang, Y. Zhang, P. Danielewicz, and M. Famiano, unpublished.
- [13] F. Sammarruca, arXiv:0807.0263 [nucl-th], and references therein.
- [14] Z.H. Li and H.-J. Schulze, Phys. Rev. C **78**, 028801 (2008).
- [15] R.B. Wiringa, V.G.J. Stocks, and R. Schiavilla, Phys. Rev. C **51**, 38 (1995).

- [16] V.G.J. Stocks, R.A.M. Klomp, C.P.F. Terheggen, and J.J. de Swart, Phys. Rev. C **49**, 2950 (1994).
- [17] S.C. Pieper, V.R. Pandharipande, R.B. Wiringa, and J. Carlson, Phys. Rev. C **64**, 014001 (2001).
- [18] C.J. Horowitz, S.J. Pollock, P.A. Souder, and R. Michaels, Phys. Rev. C **63**, 025501 (2001).